The Influences of Multiscale-Sized Second-Phase Particles on Ductility of Aged Aluminum Alloys

G. LIU, G.J. ZHANG, X.D. DING, J. SUN, and K.H. CHEN

Commercially aged aluminum alloys commonly contain second-phase particles of three class sizes, and all contribute appreciably to the mechanical properties observed at the macroscopic scale. In this article, a multiscale model was constructed to describe the individual and coupling influences of the three types of second-phase particles on tensile ductility. The nonlinear relationships between the parameters of particles, including volume fraction, size, aspect ratio, shape, and ductility, were then quantitatively established and experimentally validated by the measured results from disc-shaped precipitate containing Al-Cu-Mg alloys and needle-shaped precipitate containing Al-Mg-Si alloys, as well as by using other researchers' previously published results. In addition, we discuss extending this model to predict the fracture toughness of aluminum alloys.

I. INTRODUCTION

IN many materials, the microstructure often contains features at length scales ranging from nanometers to millimeters. The mechanical properties of materials observed at the macroscopic scale are correspondingly a type of homogenization of phenomena operating at these multilength lower scales. For the sake of quantitatively understanding how the multiscale microstructural features exert coupling effects on the mechanical properties, it is necessary to bring the detailed physics of the lower length scales up to the continuum models. This requires bridging the gaps that exist among the models and simulations at microscopic, mesoscopic, and continuum-length scales. This motivated the early multiscale material modeling that initially aimed to simulate the effects of interfaces on the macroscopic behavior of materials.[1] Subsequently, more and more interest has been focused on multiscale modeling. The areas of interest and the concerned subjects are simulating the plasticity and fracture of materials that deform and fracture at local microstructural inhomogeneity.[2,3,4] The microstructural inhomogeneity is mainly associated with the existence of void and second phase such as particles, fibers, whiskers, and so on, which, being commonly present in many materials, play very important roles in triggering the fracture process and then in determining the mechanical responses.

As the primary materials of choice for application such as in aircraft, commercially aged aluminum alloys typically show the microstructural inhomogeneity by containing three types of differently sized second-phase particles, *i.e.,* coarse ellipse-shaped constituents (from 5 to 30 μm in diameter), intermediate sphere-shaped dispersoids (from 0.02 to 0.5 μm in diameter), and fine disc- or needle-shaped strengthening precipitates (being smaller than 20 nm in the short axis).[5,6] All three types of second-phase particles make significant positive or negative contributions to the mechanical properties of aged aluminum alloys. The brittle constituents cleave or separate from the matrix during extrusion/rolling processing or under service loading to act as crack initiators or as a preferential crack propagating path. They are detrimental to ductility and fracture toughness of materials.[7] The dispersoids also directly influence crack growth and void coalescence in the deformation and fracture of material.[8] Precipitates are the major contributors to the strength of alloys. They are closely associated with the slip and deformation capability and, thus, the ductility and fracture toughness of alloys.[9]

Large numbers of qualitative experiments have been carried out to reveal the dependence of ductility and fracture toughness of aged aluminum alloys on these second-phase particles.[5,10–12] As a result, it has been well known that lowering the iron and silicon to reduce the volume fraction of constituents increases the ductility and fracture toughness of aluminum alloys.[13,14] The increase in strengthening precipitates can also reduce ductility and fracture resistance.[5] However, conflicting conclusions have been drawn about the role of dispersoids. On the one hand, it is suggested that the void sheets, which come from the decohesion of dispersoids from the matrix, truncate primary void growth and preclude a large strain accumulation decreasing the ductility and fracture toughness.[8] On the other hand, some experimental results showed that the introduction of dispersoids could promote the ductility of materials by increasing homogeneity in dislocation slip behavior.[15–18]

The most effective approach to display explicitly the independent influence and to analyze the coupled influence from every population of second-phase particles is to construct an entire model, in which quantitative relationships are revealed between ductility and the volume fractions, sizes, and shapes of the three differently sized second-phase particles. Unfortunately, the previously proposed models dealing with these relationships are exclusively based on only one scale, mostly on the scale of constituents to merely analyze the influence from constituents[5,10,12] and seldom on the scale of dispersoids to merely analyze the influence from dispersoids,[11] with failure in linking these scales. This failure can now be overcome by performing the multiscale modeling that is being developed.[2,3,4]

G. LIU and G.J. ZHANG, Doctoral Students, X.D. DING, Associate Professor, and J. SUN, Professor and Director, are with the State Key Laboratory for Mechanical Behavior of Materials, School of Materials Science and Engineering, Xi'an Jiaotong University, 710049, Xi'an, People's Republic of China. Contact e-mail: junsun@mail.xitu.edu.cn K.H. CHEN, Professor, is with the State Key Laboratory for Powder Metallurgy, University of Southern Central China, Changsha 410083, People's Republic of China.

Manuscript submitted December 10, 2002.

Although the previous multiscale models are put in practice generally using finite element (FE)–based technologies using strain gradient plasticity theory,[19,20] Green's function method,[21] and image processing,[22] jointly or separately, this article considers the coupled influences of three types of second-phase particles on ductility in an improved analytical model for aged aluminum alloys. Subsequently, we attempt to take this ductility model together with the precipitation and strengthening model previously established[23] to present an overall description of the yield strength and ductility for uniaxially tensioned aluminum alloys, which contain disc-shaped or needle-shaped precipitates, and then to validate it experimentally.

II. MODEL

In practice, it is observed that the brittle constituents will fracture readily during extrusion/rolling processing or under service loading. It is reasonable to treat them as microcracks directly (Figure 1). Assuming these microcracks arrange in a cubic array, the macrostrain to fracture of specimens, ε_f, can be obtained analytically from microplastic strain $\tilde{\varepsilon}$ as follows:[24]

$$\varepsilon_f = \frac{1}{\tilde{\varepsilon}_E(\theta)}\left[\frac{I}{0.405\pi h}\right]^{\frac{1}{n+1}}\left[\frac{\lambda_c}{2r_c}-1\right]^{\frac{1}{n+1}}\frac{\tilde{\varepsilon}}{2} \qquad [1]$$

where λ_c and r_c are interparticle spacing and radius of constituents, respectively; $\tilde{\varepsilon}_E(\theta)$ is the effective value for the normalized coefficient $\tilde{\varepsilon}_{ij}(\theta)$ and is a constant for $\theta = 0$; and I and h are functions of the strain-hardening exponent n.[25,26] The $\tilde{\varepsilon}$ is critical local strain at the middle of the ligament connecting the two most neighboring microcracks. It is also equivalent to the minimum strain needed for inducing the void or microcracks growing and coalescing to instability. The dispersoids and precipitates distributed in the ligament dominate this damage evolution process.

In the uniaxil tensile condition, the incompatibility in shape change between the aluminum matrix and dispersoids and precipitates incurs geometrically necessary dislocations introduced to make up for the discrepancy.[27] The densities of geometrically necessary dislocations around the sphere-shaped dispersoids and disc- or needle-shaped precipitates, ρ_d and ρ_p, are closely decided by the strains exerted on the adjacent matrix bonded with the two populations of particles, ε_d and ε_p, respectively:[27,28]

$$\varepsilon_d = 1.7 r_d \mathbf{b}\,\rho_d \qquad [2a]$$

$$\varepsilon_p = 0.25\lambda_p \mathbf{b}\,\rho_p \qquad [2b]$$

with r_d being the radius of dispersoids, λ_p being the interparticle spacing of precipitates, and **b** being the Burgers vector of the matrix. According to Ashby,[27] the ratio between ρ_d and ρ_p is associated with the ratio between interparticle spacings of the two populations of particles, λ_d and λ_p, as follows:

$$\frac{\rho_d}{\rho_p} = k\frac{\lambda_p}{\lambda_d} \qquad [3]$$

where k is a scaling factor and considered as unity here. Letting ρ_g be the sum of ρ_d and ρ_p, it plus the density of statistically stored dislocations, ρ_s, comes to the total dislocation density in the matrix, ρ_t:

$$\rho_t = \rho_g + \rho_s \qquad [4]$$

A critical value of ρ_t, denoted as ρ_t^c, is assumed to exist. When the total dislocation density of ρ_t excesses the "dislocation limit" of ρ_t^c, the material fractures immediately. Neglecting constraint from second-phase particles, ρ_t^c should be a constant by hypothesizing that the following engineering mechanical expression can apply effectively in the microscale of the ligament:

$$\tau_m = \alpha G\mathbf{b}\sqrt{\rho_t^c} \qquad [5]$$

where τ_m, the intrinsic shear strength of the matrix, G, the shear modulus of matrix, together with b and α are all constants for a given matrix such as aluminum. At the same time, ρ_s can be approximately considered invariant because the increase in ρ_s is inappreciable compared with that in ρ_g under external loading.[29] Therefore, the criterion for fracture is further defined as ρ_g reaching the constant ρ_g^c:

$$\rho_g^c = \rho_t^c - \rho_s \qquad [6]$$

From aforementioned analyses, Eq. [2] could be rewritten as

$$\varepsilon_d^c = 1.7 r_d \mathbf{b}\frac{\lambda_p}{\lambda_d+\lambda_p}\rho_g^c \qquad [7a]$$

$$\varepsilon_p^c = 0.25\lambda_p \mathbf{b}\frac{\lambda_d}{\lambda_d+\lambda_p}\rho_g^c \qquad [7b]$$

The microplastic strain of $\tilde{\varepsilon}$ in Eq. [1] is a combination of ε_d^c and ε_p^c in the form of the Pythagorean theorem, not of linear addition due to the existence of the overlap effect between the two types of strains:

$$\tilde{\varepsilon} = \sqrt{(\varepsilon_d^c)^2 + (\varepsilon_p^c)^2} \qquad [8]$$

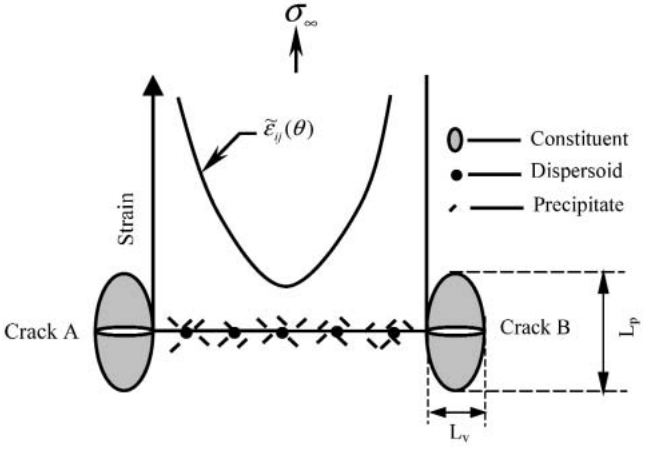

Fig. 1—Sketch illustrating the local fracture behavior in heat-treatable aluminum alloys containing three types of second-phase particles.

So the strain to fracture or tensile ductility of aluminum alloys can be obtained as

$$\varepsilon_f = \frac{\mathbf{b}\rho_g^c}{2\tilde{\varepsilon}_E(\theta)}\left[\frac{I}{0.405\pi h}\right]^{\frac{1}{n+1}}\left[\frac{\lambda_c}{2r_c}-1\right]^{\frac{1}{n+1}}(\lambda_d+\lambda_p)^{-1}\sqrt{[(1.7r_d\lambda_p)^2+(0.25\lambda_d\lambda_p)^2]} \quad [9]$$

If the three types of second-phase particles are all assumed as be in cubic arrangement, the relationships among the parameters, *i.e.,* volume fraction f_i ($i = c, d, p$), mean radius r_i, mean interparticle spacing λ_i, and aspect ratio k_i, of second-phase particles should be

$$f_i = c\pi k_i (r_i/\lambda_i)^3 \quad [10]$$

with the constant c being equal to 2 for constituents and precipitates and 4/3 for dispersoids. The aspect ratio of ellipse-shaped constituents, k_c, is artificially defined in Figure 1. This defined k_c is equal to the actual aspect ratio when the external loading axis is parallel to the longer axis of constituents, whereas k_c is equivalent to the reciprocal of the actual aspect ratio when the external loading axis is parallel to the short axis of constituents.

The result of combining Eqs. [9] and [10] explicitly shows the independent and combined influences from three types of second-phase particles on the tensile ductility of aged aluminum alloys. Furthermore, because the parameters of precipitates vary with aging time, the relationship between tensile ductility and aging time is established as well. In order to clearly show the variation of ductility with any parameter of second-phase particles or aging time, a referred ductility, $(\varepsilon_f)_R$, is chosen as the standard and this variation can be simply reflected as the variation of the normalized ductility, R_N, which is the ratio between the ductility with the parameter varying and the referred ductility:

$$R_N = \varepsilon_f/(\varepsilon_f)_R \quad [11]$$

In the following calculations, if Eq. [11] is used to predict the evolution of ductility with second-phase particles, the $(\varepsilon_f)_R$ is chosen as the ductility when there are no second-phase particles and the ε_f represents the ductility when there are increasing second-phase particles. If Eq. [11] is used to predict the evolution of ductility with aging, the $(\varepsilon_f)_R$ is chosen as the ductility of as-quenched material and the ε_f represents the ductility of material in aging. All of these definitions are displayed in the following figures.

III. EXPERIMENTAL PROCEDURE

A. *Materials and Processing*

Although the present model reveals the relationships between the tensile ductility and the parameters of three types of second-phase particles in aged aluminum alloys, we cannot validate all of these relationships in the present experiment because the materials used in this experiment were supplied as extruded rods. The chemical composition and fabrication process have presented predefined distributions of constituents and dispersoids, which are hardly changed by subsequent heat treatments. We can only change the parameters of precipitates by using aging treatment. Therefore, in the present experiment, only the predicted influence of precipitates on ductility could be well verified. Some other researchers' relevant experimental results must be used when the predicted influences of constituents and dispersoids on ductility are involved.

Two types of aluminum alloys, containing Al-Cu-Mg (AA2xxx, abbreviated as Al-Cu-Mg alloy) and Al-Mg-Si (AA6xxx, abbreviated as Al-Mg-Si alloy), respectively, were supplied by the Research Laboratory of Xi'an Air Craft Industry Ltd., (Xi'an, China) for use in this experiment. The chemical composites of the two types of alloys are list in Table I. The heat treatments of Al-Cu-Mg and Al-Mg-Si alloys include solution treating at 766 K for 2 hours and at 703 K for 30 minutes, followed by water quenching and subsequent aging at 513 and 463 K for various times from 0.25 hours to 10 days.

B. *Microstructural Evaluation*

The microstructures of sectioned Al-Cu-Mg and Al-Mg-Si rods were examined using optical microscopy. Metallographic preparation involved methods of standard surface preparation. The specimens were etched with Keller's etchant.

The volume fraction of coarse constituent was measured at a magnification of 400 times by using point counting with a grid containing 900 points. Six random views on each of three specimens per alloys were examined. The distribution of the constituents within each alloy was regarded as random; therefore, the volume fraction, V_c, is given by P_p, which is the fraction of total grid points that fall on constituent particles. Constituents smaller than 0.1 μm were not counted.

Using a Hitachi* S-2700 scanning electron microscope, the size measurements of the constituents were performed on sectioned profiles of the untested specimens. Since the constituents are irregular in shape, an effective particle diameter, d_c, was defined as

*HITACHI is a trademark of Hitachi Ltd., Japan.

$$d_c = \sqrt{d_1 d_2} \quad [12]$$

where d_1 and d_2 are the smallest and largest dimensions of a coarse constituent, respectively. Regardless of the anisotropy of the constituents, the mean radius, $\bar{r}_c$, of n particles is then given by

$$\bar{r}_c = \left(\sum_{i=1}^{n}\sqrt{d_1 d_2}\right)/2n \quad [13]$$

To obtain the accurate value of $\bar{r}_c$ for each alloy, at least 50 constituents were measured in each of three sectioned specimens.

The dispersoid radius was determined by the same treatments in a JEOL* Ltd. JEM-200CX transmission electron

*JEOL is a trademark of Japan Electron Optics Ltd., Tokyo.

Table I. Chemical Composition in Weight Percent

Alloys	Cu	Mg	Si	Mn	Cr	Fe	Zn	Al
Al-Cu-Mg	4.62	0.65	<0.3	0.22	—	<0.3	<0.3	balance
Al-Mg-Si	0.25	1.12	0.57	—	0.22	—	—	balance

microscope operating at 100 kV. The volume fraction of dispersoids is related to the average effective radius as[30]

$$V_d = \frac{4}{3}\pi \bar{r}_d^3 \bar{N}_d \quad [14]$$

The particle density $\bar{N}_d$ is defined as[31]

$$\bar{N}_d = \frac{N_d}{(h + 2\bar{r}_d)} \quad [15]$$

where h is the foil thickness and is easily obtained using convergent beam electron diffraction patterns,[32] and N_d is the number of dispersoids per unit area of projected image.

C. *Mechanical Testing*

At room temperature, dog-bone-shaped tensile specimens from both alloys, having a gage size of 6 mm in diameter and 40 mm in length, were tested at a constant strain rate of $5 \times 10^{-4}\ s^{-1}$ on a servohydraulic Instron* 1346 testing machine. The load direction is parallel to the rod axis. Yield strength (0.2 pct offset) (σ_{ys}), tensile strength (σ_{uts}), strain-hardening exponent at necking, and tensile ductility or strain to fracture $\varepsilon_f = \ln (A_0/A_f)$ (A_0: initial area, and A_f: area at fracture) were measured for every specimen.

*INSTRON is a trademark of Instron Corp., Canton, MA.

IV. RESULTS

A. *Grain Structure*

Optical metallography of the two alloys revealed large, pancake-shaped grain structures; the grain size is approximately 1200-μm long by 100-μm wide for Al-Cu-Mg alloys and 700-μm long by 50-μm wide for Al-Mg-Si alloys, as illustrated in Figure 2.

B. *Parameters of Constituents and Dispersoids*

The measured volume fraction and size of coarse constituents and intermediate dispersoids in Al-Cu-Mg and Al-Mg-Si alloys are summarized in Table II, and the typical micrographs of constituents and dispersoids in the two alloys are shown in Figures 3 and 4, respectively.

C. *Evolution of Precipitates*

Figure 5 displays the evolution of precipitates in size during aging, for the two alloys, separately. As for the variation of size of precipitates, it was measured that, at the underaged stage, both the diameter of the disc-shaped precipitates (Figure 6(a)) in Al-Cu-Mg alloys and the length of the needle-shaped precipitates (Figure 6(b)) in Al-Mg-Si alloys were directly proportional to the square root of aging time, t (seconds). However, at the overaged stage, the dimensions of the coarsening precipitates in Al-Cu-Mg and Al-Mg-Si alloys followed the $t^{1/5}$ and $t^{1/4}$ law, respectively; *i.e.,*

$$\text{for Al-Cu-Mg alloys,} \qquad r_p = 25.64 \times t^{1/5} \quad [16a]$$

and

$$\text{for Al-Mg-Si alloys,} \qquad l_p = 2.69 \times t^{1/4} \quad [16b]$$

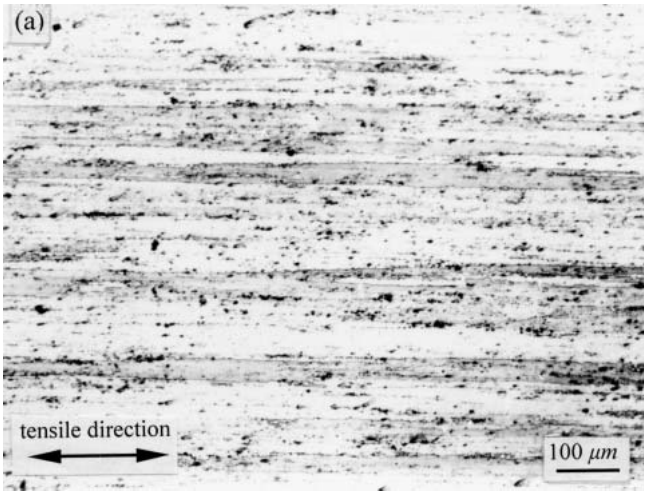

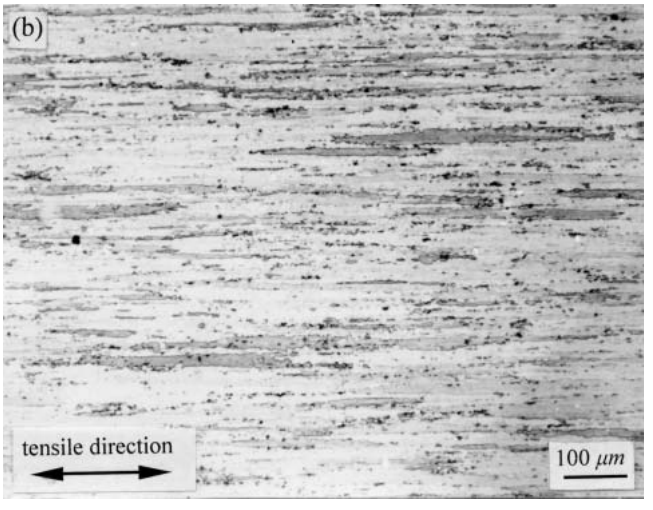

Table II. Parameters of Constituents and Dispersoids

Alloys	f_c/Vol Pct	r_c/μm	k_c^*	f_d/Vol Pct	r_d/μm	k_d
Al-Cu-Mg	4.83	4.1	3.2	0.18	0.08	1.1
Al-Mg-Si	3.46	2.4	2.1	0.11	0.03	1.2

*Actual aspect ratio.

The variation of the measured aspect ratio and volume fraction of the two types of precipitates with aging time and the micrographs for typically demonstrating the dimensional evolution and morphological evolution of precipitates with aging time in the two alloys have been shown and are discussed in detail elsewhere.[23]

D. *Tensile Properties*

The influence of aging on tensile properties of the two alloys is summarized in Table III. It is found that, contrary to the variation of strength with aging, the tensile ductility

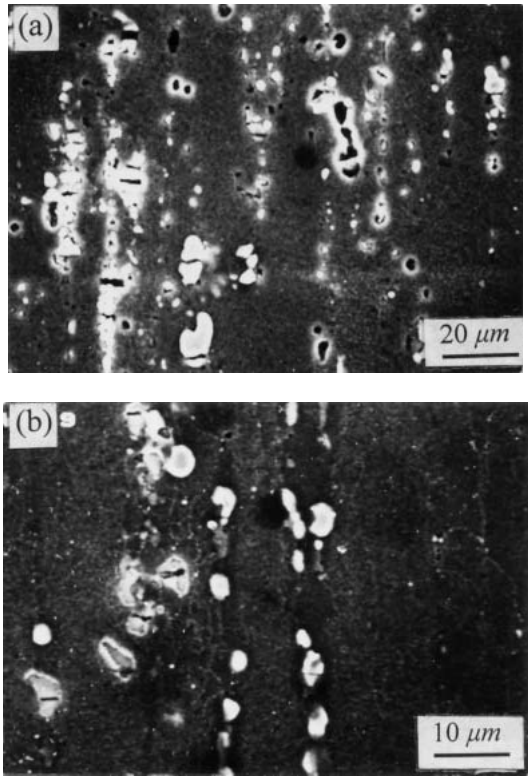

Fig. 3—SEM micrographs typically showing the morphology and size of constituents in (*a*) Al-Cu-Mg alloys and (*b*) Al-Mg-Si alloys.

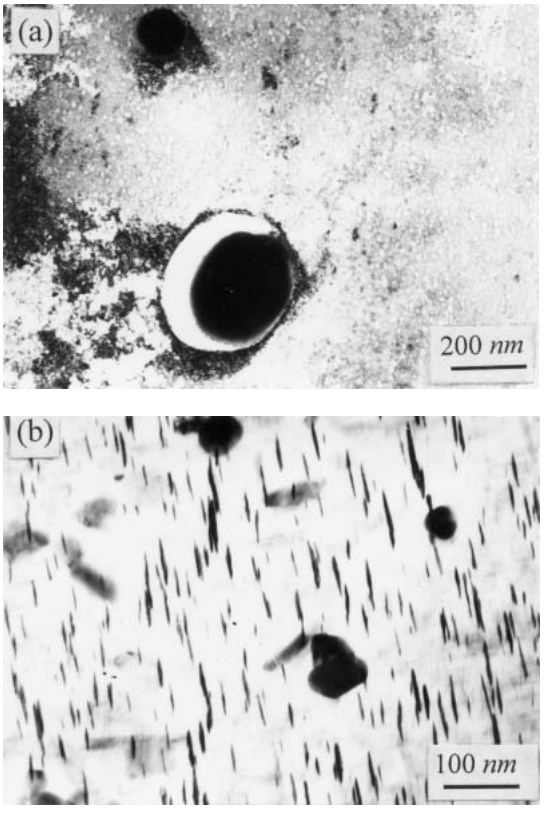

Fig. 4—TEM micrographs typically showing the morphology and size of dispersoids in (*a*) Al-Cu-Mg alloys and (*b*) Al-Mg-Si alloys.

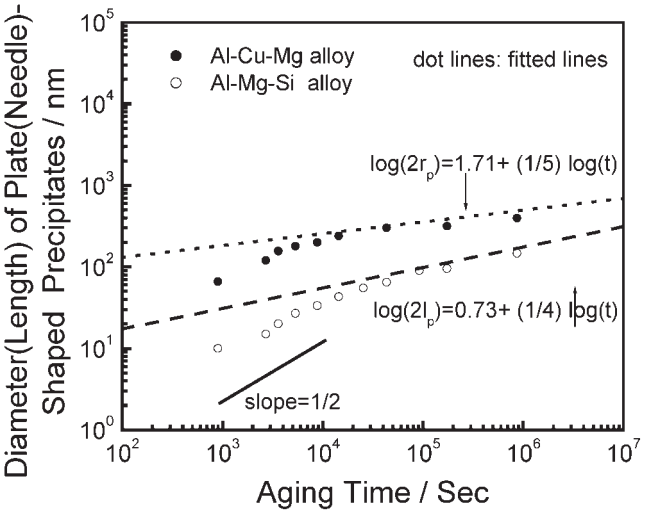

Fig. 5—Variation of principal dimensions of precipitates (diameter for disc-shaped precipitates and length for needle-shaped precipitates) with aging process in Al-Cu-Mg alloys aged at 513 K and Al-Mg-Si alloys aged at 463 K.

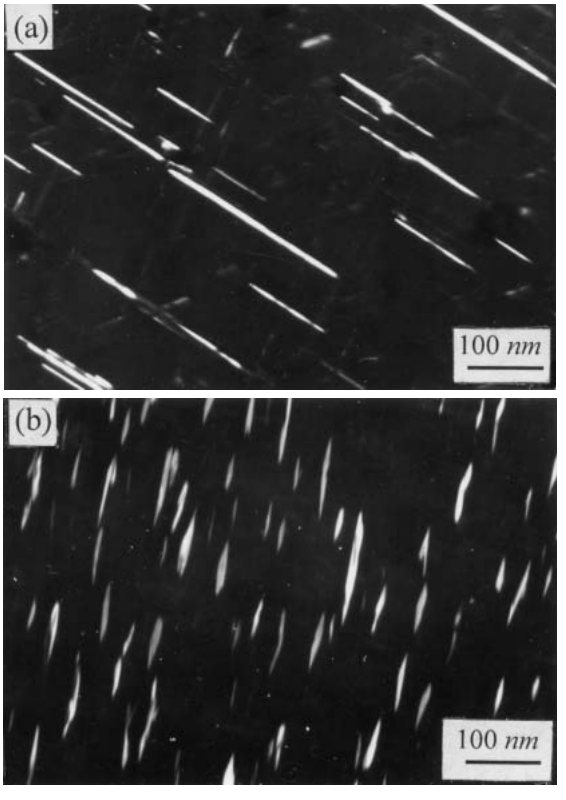

Fig. 6—TEM dark-field micrographs typically showing the morphology of (*a*) disc-shaped precipitates in Al-Cu-Mg alloys and (*b*) needle-shaped precipitates in Al-Mg-Si alloys.

decreases from the underaged condition to the peak-aged state and then increases again at the overaged stage, which has been observed in other researchers' experiments on progressively aged aluminum alloys.[9,10,33–35]

Table III. Summary of Tensile Properties

Alloys	t/s	σ_{ys}/MPa	σ_{utx}/MPa	ε_f/Pct	n
Al-Cu-Mg	9.00×10^2	205	263	34.0	0.23
(aged at	2.70×10^3	259	308	30.0	0.21
513 K)	3.60×10^3	291	340	28.5	0.17
	5.40×10^3	303	349	27.8	0.14
	9.00×10^3	289	337	28.1	0.13
	1.44×10^4	273	328	28.8	0.16
	4.32×10^4	245	302	31.7	0.20
	1.73×10^5	228	284	34.2	0.24
	8.64×10^5	213	270	35.9	0.29
Al-Mg-Si	9.00×10^2	151	227	36.5	0.35
(aged at	2.70×10^3	173	238	32.2	0.30
463 K)	3.60×10^3	189	246	31.0	0.26
	5.40×10^3	197	257	27.9	0.24
	9.00×10^3	221	276	26.6	0.22
	1.44×10^4	240	295	25.6	0.25
	2.52×10^4	259	313	23.8	0.27
	4.32×10^4	253	310	25.2	0.33
	9.16×10^4	247	301	26.0	0.34
	1.73×10^5	238	293	27.4	0.38
	8.64×10^5	226	288	30.9	0.43

V. DISCUSSION

A. *The Influence of Constituents on Ductility*

1. *Volume fraction of constituents*

Keeping the volume fraction and size of dispersoids and precipitates constant, the influence of the volume fraction of constituents on ductility can be modeled from Eqs. [9] and [10] combined with Eq. [11] by defining the $f_c = 0$ as referred standard and by changing the aspect ratio of constituents, as shown in Figure 7. The corresponding experimental results from Walsh *et al.*,[18] drawn in the identical figure, are found to be in broad agreement with the modeled counterparts.

It is delineated from Figure 7 that increasing the volume fraction of constituents sharply reduces the ductility of aluminum alloys, and, especially, when the volume fraction is increased to 1 pct, only half of the intrinsic ductility survives. This trend is not only observed in aluminum alloys,[5,7,36] but also exists commonly in other metals and alloys that contain nonmetallic inclusions.[37,38] In particular, the fitted functional relationship of the volume fraction of inclusions and tensile ductility in copper[39] is nearly the same as the present modeled curves for aluminum alloys.

Many efforts typically based on the Thomason model have been dedicated to modeling the effect of volume fraction of inclusions/voids on ductility.[40,41,42] A new equation was proposed by Komori[41] to relate the ductility to the volume fraction of voids, f_c, as

$$\varepsilon_f = \ln\left[-\frac{1}{2} + \sqrt{\left(\frac{1}{\sqrt{f_c}} - \frac{1}{2}\right)}\right] \qquad [17]$$

However, the predicted results from Eq. [17] are essentially consistent with the present modeled results (Figure 7).

2. *Aspect ratio of coarse constituents*

After extrusion or rolling processing, the coarse constituents in processed aluminum alloys are usually in the ellipse shape with the larger axis being parallel to the extrusion or roll direction. In the subsequent tensile condition, when the loading axis is parallel to the larger axis of constituents, the defined aspect ratio of constituents is greater than unity (Figure 8(a)); when the loading axis is parallel to the shorter axis of constituents, the defined aspect ratio of constituents is smaller than unity (Figure 8(b)). According to the simulated results in Figure 7, the ductility in the latter case is inferior to that in the former case, because the ligament between two most neighboring constituents/voids is shorter in the latter case, and the shorter ligament implies an ease in coalescing the two voids and a lower capacity in resisting deformation.

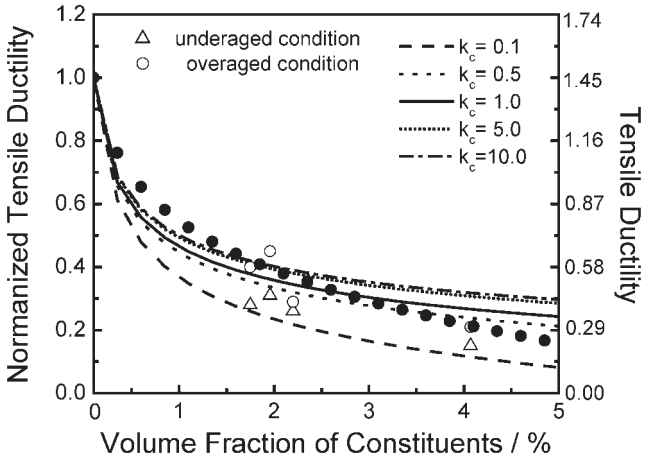

Fig. 7—The modeled dependence (lines) of tensile ductility on volume fraction and aspect ratio of constituents compared with results (closed dots) of modified Thomason model[41] and some measured values (open dots) from Ref. 18.

3. *Size and characteristics of constituents*

It has been experimentally observed that there was no effect of inclusion size on tensile ductility for the weakly bonded particles.[39] Similarly, this would be applicable for the readily broken constituents, which fits well with the inference from Eq. [9] combined with Eq. [10]. In addition, the constituents are apt to cleave during extrusion/rolling processing; therefore, they can be directly considered as voids in modeling construction. But, if most constituents do not cleave and do not turn into voids during the extrusion/rolling processing, the strain for nucleating voids at constituents, ε_v, should be included in the total tensile ductility in modeling construction. This means that the total tensile ductility, ε_f^T, is the sum of ε_f in Eq. [9] and ε_v:

$$\varepsilon_f^T = \varepsilon_f + \varepsilon_v = \frac{1}{\tilde{\varepsilon}_E(\theta)}\left[\frac{I}{0.405\pi h}\right]^{\frac{1}{n+1}}\left[\frac{\lambda_c}{2r_c} - 1\right]^{\frac{1}{n+1}} \frac{\sqrt{(\varepsilon_d^c)^2 + (\varepsilon_p^c)^2}}{2} + \varepsilon_v \qquad [18]$$

About ε_v, many expressions have been derived on the basis of energy balance for interfacial decohesion between particles and matrix,[38,42–44] and it is more advisable that ε_v is associated not only with the size of constituents but also with the characteristics of constituents, for example, as[42]

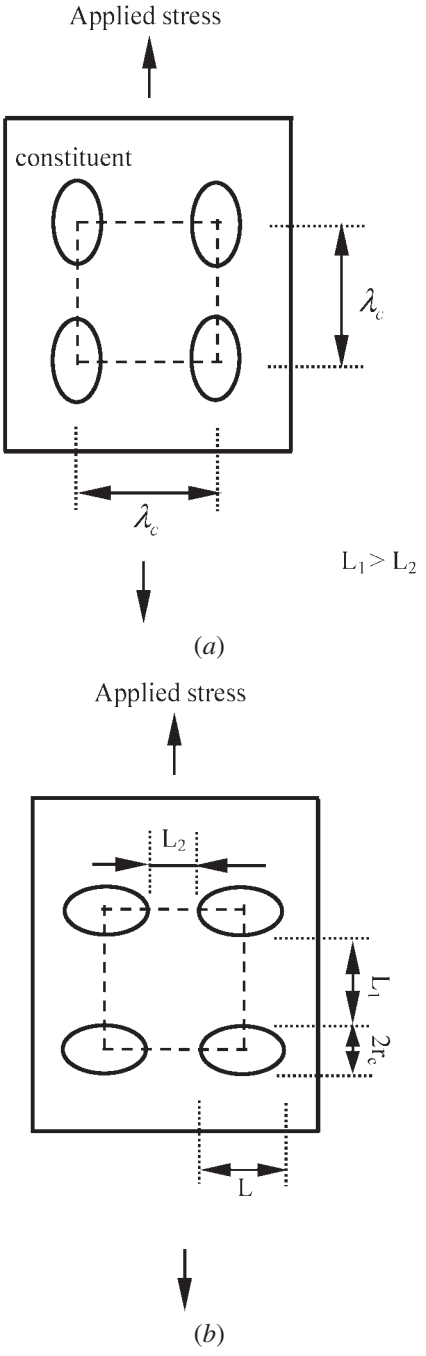

Fig. 8—Sketch illustrating the contribution of constituent arrangement to the orientation effect of extruded or rolled aluminum alloys in tensile ductility with applied stress being (*a*) parallel or (*b*) vertical to the extrusion or rolling direction.

$$\varepsilon_v = \left(\frac{G\mathbf{b} + G_c\mathbf{b}_c}{1.67\, E_c r_c} \right)^{1/2} \qquad [19]$$

where G and G_c are, respectively, the shear modulus of matrix and the constituents; $\mathbf{b}$ and $\mathbf{b}_c$ are the Burgers vectors, respectively; and E_c is the Young's modulus of constituents. Equation [19] clearly shows that the constituents that are larger (greater r_c) as well as more incompatible with the matrix in characteristics (smaller G/E_c) are more prone to be turned into voids under service loading.

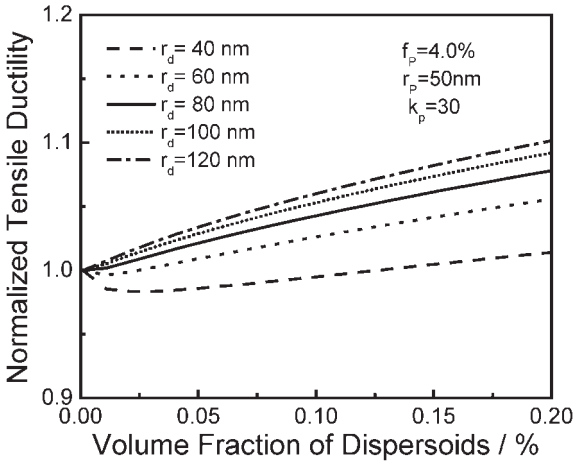

Fig. 9—The modeled dependence of tensile ductility on volume fraction and size of dispersoids.

B. *The Influence of Dispersoids on Ductility*

1. *Volume fraction of dispersoids*

Figure 9 explicitly shows the dependence of ductility on the volume fraction of dispersoids. As the modeled results in Figure 9 shows the introduction of some dispersoids is favorable for improving ductility. This conclusion is supported by many experimental results, where the fracture mode is modified by suppressing intergranular fracture and promoting transgranular fracture after introducing some dispersoids.[15–18] This modification of fracture mode is believed to be the result of refining grain size as well as homogenizing slip behavior.[15–18] However, another possible mechanism may be responsible for this modification; *i.e.,* the introduction of some dispersoids triggers the formation of void sheets by interfacial debonding (Figure 4(a)) and then promotes transgranular fracture. It then can be concluded that the introduction of some dispersoids slightly lowers the energy required for transgranular fracture and so increases the percent of transgranular fracture. However, the volume fraction of dispersoids should be limited because too many dispersoids are sure to degrade the deformation capacity. A high density of small dispersoids can lead to a high density of voids that form void sheets and localized deformations. This effect dramatically reduces macroscopic ductility.

2. *Size of dispersoids*

Dispersoids can be coarsened by industrial heat treatment and this increases dispersoid spacing. The increased dispersoid spacing increases the void spacing, which can promote the ductility (Figure 9) as long as the dispersoids are not so large to induce early void nucleation. This predicted result in Figure 9 has been observed in some previous experiments[45,46] in which ductility was increased by enlarging the size of dispersoids, and this trend may be due to the fact that the coarsening of dispersoids can make decohesion easier and promotes transgranular fracture.

C. *The Influence of Precipitates on Ductility*

1. *Volume fraction of precipitates*

As the major contributors for strength of aged aluminum alloys, the precipitates bring about more possibilities of strain

localization. This finding suggests that the variation of ductility is generally opposite to that of strength in the course of aging. Accordingly, the ductility is destined to degrade by adding the amount of strengthening precipitates, which is quantitatively depicted by this model, as in Figure 10. This is identical to the regularity that the material possessing greater strength commonly exhibits less ductility.

The experimentally measured ductility variations of aged alloys containing Al-Cu-Mg and Al-Mg-Si with volume fraction of precipitates are drawn in Figure 10. These results reveal that, at the underaged stage, ductility decreases monotonically for the two alloys, because the volume fraction of precipitates increases up to peak-aged condition. However, at the overaged stage, the ductility increases gradually, and this rebound is associated with the enlarging in size of precipitates under a constant volume fraction.

2. *Size and characteristic of precipitates*

At peak aging condition, the excess precipitate-forming solute atoms are exhausted from the matrix and the volume fraction of precipitates is constant. The main evolution of precipitates at this time is the coarsening in size *via* Ostwald ripening, which results in a decrease in strength with an increase in ductility, just as the present experiments demonstrate. Although precipitates coarsen in the underaged condition, the increase in volume fraction of precipitates plays a dominant role so that ductility decreases instead of increasing. The dominant influence of volume fraction over dimension is explicitly described by the modeled curves in Figure 10.

Similarly, the effects of various types of precipitates on ductility are closely related to the strengthening responses of the different precipitates. When the precipitates have a strong strengthening response, they exert a serious detrimental influence on the ductility, and *vice versa.* As a result, the precipitates should be suitably controlled in order to obtain a optimal combination of both the ductility and the strength.

3. *Aging time*

The variation of the ductility with aging time for the two alloys is presented in Figure 11. The curves are obtained by substituting the parameters of constituents and dispersoids in Table II, as well as those of precipitates from Liu *et al.*[23] into the Eqs. [9] and [10] and using Eq. [11]. Figure 11 shows that the measured values agree well with the modeled curves, which validates the applicability and feasibility of this model for aged aluminum alloys containing either disc-shaped precipitates or needle-shaped precipitates.

D. *The Coupled Influences of Second-Phase Particles*

The influence of second-phase particles on ductility was discussed previously as resulting from changing the parameters of only one type of second-phase particles and holding constant those of the other two types. The interaction of all of these can be clearly revealed if the parameters of two or three types of second-phase particles are varied simultaneously.

1. *Constituents and precipitates*

Figure 12 shows the variation of ductility with the trade-off in volume fraction of constituents and precipitates by fixing the total content of the two types of particles as 5 vol pct. The main conclusions on reduced ductility are that constituents are more detrimental than precipitates. If the formation of constituents

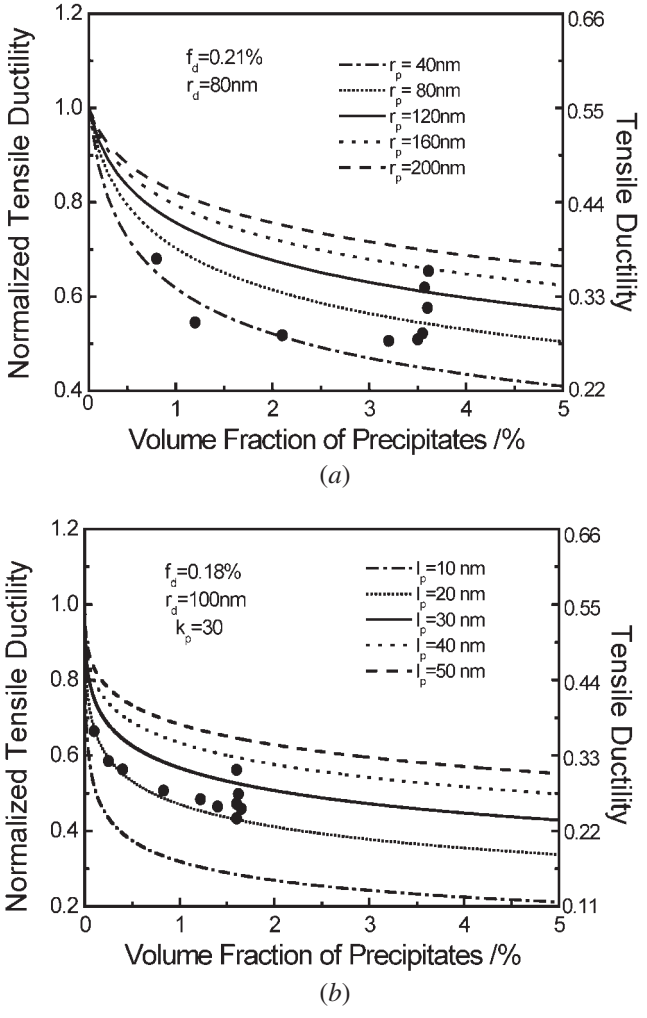

Fig. 10—The modeled dependence of tensile ductility on volume fraction and size of precipitates compared with the measured values (*a*) of Al-Cu-Mg alloys and (*b*) of Al-Mg-Si alloys.

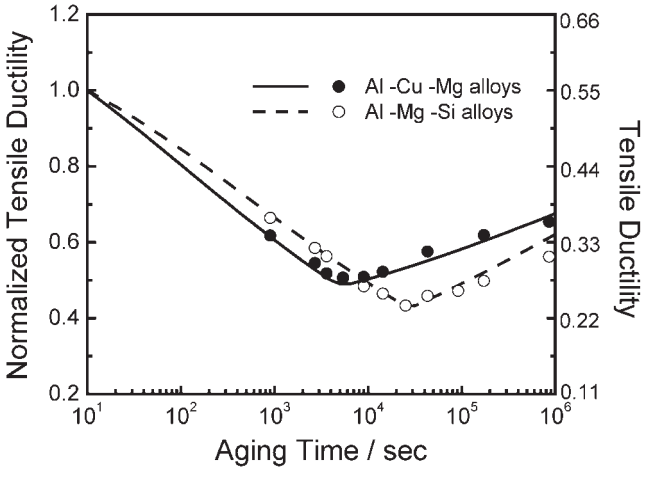

Fig. 11—The modeled variation of tensile ductility with aging process compared with the measured values of Al-Cu-Mg alloys aged at 513 K and Al-Mg-Si alloys aged at 463 K.

containing precipitate-forming elements can be suppressed, the ductility can be improved because the more detrimental constituent phase particle are decreased.

2. *Precipitates and dispersoids*

Figure 13 shows the variation of ductility with precipitates as the volume fraction of dispersoids changes. Precipitates reduce ductility less as the volume fraction of dispersoids increases. The effect is relatively small in these alloys and the effect of precipitates dominates.

E. *Simulating Fracture Toughness from the Present Model*

Based on the criterion that fracture will occur when the local strain ahead of the main crack exceeds the critical value, ε_c^* , an expression has been established to relate the fracture toughness of high-strength aluminum alloys to the yield strength, the strain-hardening exponent, the Young's modulus, E, and ε_c^*:[10]

$$K_{IC} = \sqrt{\frac{2CE\varepsilon_c^*\sigma_{ys}\, n^2}{(1-\upsilon^2)}} \qquad [20]$$

where C is a constant of ~1/40 and υ is the Poisson ratio. Because ε_c^* has been suggested to be in proportion to ε_f by a factor of F[47,48,49] and for aged aluminum alloys, F can be taken as 1/2,[10] Eq. [9] can be directly substituted into Eq. [20] with the result

$$K_{IC} = \Gamma \sqrt{Bn^2\sigma_y \left[\frac{\lambda_c}{2r_c} - 1\right]^{\frac{1}{n+1}} [(1.7\, r_d\lambda_p)^2 + (0.25\lambda_p\lambda_d)^2]^{1/2} (\lambda_d + \lambda_p)^{-1}} \qquad [21]$$

with

$$\Gamma = \sqrt{\frac{CE\mathbf{b}\rho_g}{2\tilde{\varepsilon}_n(\theta)}} \qquad [22]$$

and

$$B = [(1 + 3n)(5.39\sqrt{0.13 + n} - 2.53n)^{[1/(n+1)]} \qquad [23]$$

Equation [21] relates the fracture toughness to parameters of the three types of second-phase particles in a nonlinear manner. Especially, Eq. [21] could be simply written as

$$\frac{K_{IC}}{\sqrt{\sigma_{ys}E}} \propto \left[\frac{\lambda_c}{2r_c} - 1\right]^{\frac{1}{2(n+1)}} \qquad [24]$$

or

$$\frac{K_{IC}}{\sqrt{\sigma_{ys}E}} \propto \left[\left(\frac{\pi k_c}{4f_c}\right)^{1/3} - 1\right]^{1/[2(n+1)]} \qquad [25]$$

The results regarding the dependence of K_{IC} on the constituent content from Eq. [25] cover that by Hahn and Resenfoeld,[5] who proposed the well-validated relationship of $K_{IC}/\sqrt{\sigma_{ys}E} \propto f_c^{-1/6}$, as in Figure 14.

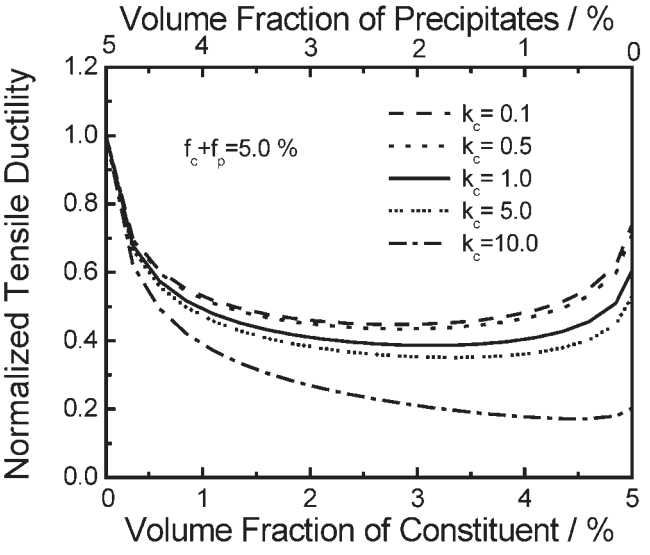

Fig. 12—The modeled coupling influences of constituents and precipitates on tensile ductility with the trade-off in contents of constituents and precipitates by fixing the total content of the two particles as 5 vol pct (f_d = 0.21 pct, r_d = 80 nm, k_p = 30, and r_p = 100 nm).

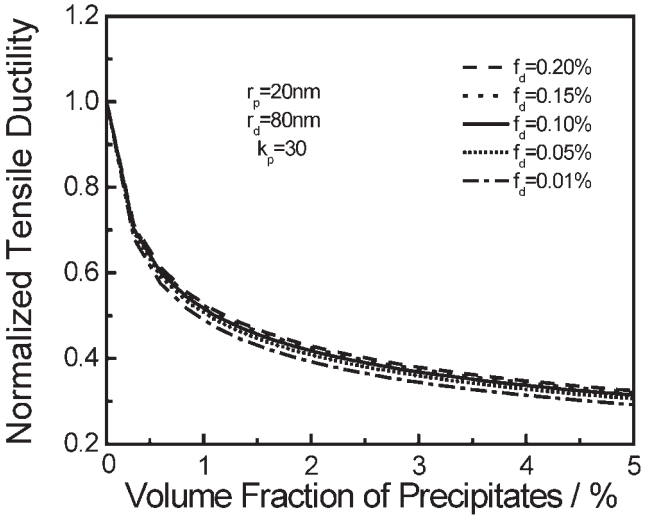

Fig. 13—The modeled coupling influences of precipitates and dispersoids on tensile ductility with the precipitate and dispersoid contents being changed.

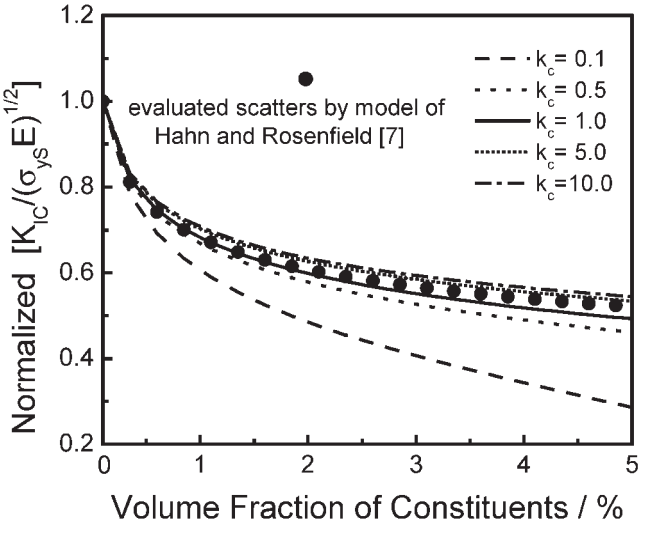

Fig. 14—The modeled dependence of fracture toughness on volume fraction and aspect ratio of constituents compared with that from the model in Ref. 5.

VI. CONCLUSIONS

1. Based on the present multiscale modeling, the independent and combined influences of second-phase particles of three classes of size on ductility for aged aluminum alloys have been quantitatively shown. In addition, a multiscale model for fracture toughness was constructed using the present ductility model.
2. The hardening precipitates not only enhance strength but also degrade ductility, and the stronger the hardening effect from precipitates, the more the ductility decreases. However, constituents have a far greater detrimental effect than do precipitates.
3. The variations of ductility with aging time for disc-shaped-precipitate–containing Al-Cu-Mg alloys aged at 513 K and needle-shaped-precipitate–containing Al-Mg-Si alloys aged at 463 K were measured and broadly modeled.

ACKNOWLEDGMENTS

The financial support from the State Key Project of Fundamental Research of China (Grant No. G1999064909) is sincerely acknowledged. The authors express their special thanks for the support from the National Natural Science Foundation of China and the National Outstanding Young Investigator grant of China. The valuable comments and kind suggestions from reviewers are also sincerely appreciated.

REFERENCES

1. W.E. King, G. Campbell, T. Gonis, G. Henshall, D. Lesuer, E. Zywicz, and S. Foiles: *Mater. Sci. Eng. A,* 1995, vol. A191, pp. 1-16.
2. G.H. Campbell, S.M. Foiles, H. Huang, D.A. Hughes, W.E. King, D.H. Lassila, D.J. Nikkel, T.D. Rubia, J.Y. Shu, and V.P. Smyshlyaev: *Mater. Sci. Eng. A,* 1998, vol. A251, pp. 1-22.
3. A.M. Gokhale and S. Yang: *Metall. Mater. Trans. A,* 1999, vol. 30A, pp. 2369-81.
4. Z. Xia, W.A. Curtin, and P.W.M. Peters: *Acta Mater.,* 2001, vol. 49, pp. 273-87.
5. G.T. Hahn and A.R. Rosenfield: *Metall. Metall. Trans. A,* 1975, vol. 6A, pp. 653-68.
6. D.S. Thompson: *Metall. Trans. A,* 1975, vol. 6A, pp. 671-83.
7. D. Broek: *Eng. Fract. Mech.,* 1973, vol. 5, pp. 55-66.
8. R.H. Van Stone, T.B. Cox, J.R. Low, JR., and J.A. Psioda: *Int. Met. Rev.,* 1985, vol. 30, pp. 157-79.
9. K.V. Jata and E.A. Starke, Jr.: *Metall. Trans. A,* 1986, vol. 17A, pp. 1011-26.
10. G.G. Garrett and J.F. Knott: *Metall. Trans. A,* 1978, vol. 9A, pp. 1187-200.
11. C.Q. Chen and J.F. Knott: *Met. Sci.,* 1981, vol. 15, pp. 357-64.
12. M. Nakai and T. Eto: *Mater. Sci. Eng. A,* 2000, vol. A285, pp. 62-68.
13. J.G. Kaufman, P.E. Schilling, and F.G. Nelson: *Met. Eng. Q.,* 1969, vol. 9, pp. 39-47.
14. J.T. Staley: *ASTM STP605,* ASTM, Philadelphia, PA, 1975, pp. 71-103.
15. J.M. Dowling and J.W. Martin: *Acta Metall.,* 1976, vol. 24, pp. 1147-53.
16. K.C. Prince and J.W. Martin: *Acta Metall.,* 1979, vol. 27, pp. 1401-08.
17. J.A. Blind and J.W. Martin: *Mater. Sci. Eng.,* 1983, vol. 57, pp. 49-54.
18. J.A. Walsh, K.V. Jata, and E.A. Starke, Jr.: *Acta Metall.,* 1989, vol. 37, pp. 2861-71.
19. N.A. Fleck and J.W. Hutchinson: *J. Mech. Phys. Solids,* 1993, vol. 41, pp. 1825-57.
20. H. Gao, Y. Huang, W.D. Nix, and J.W. Hutchinson: *J. Mech. Phys. Solids,* 1999, vol. 47, pp. 1239-63.
21. S.J. Zhou and W.A. Curtin: *Acta Metall. Mater.,* 1995, vol. 43, pp. 3093-104.
22. A. Tewari, A.M. Gokhale, and R.M. German: *Acta Mater.,* 1999, vol. 47, pp. 3721-34.
23. G. Liu, G.J. Zhang, X.D. Ding, J. Sun, and K.H. Chen: *Mater. Sci. Eng. A,* 2003, vol. 344, pp. 113-24.
24. K.S. Chan: *Acta Metall. Mater.,* 1995, vol. 43, pp. 4325-35.
25. J.R. Rice and G.F. Rosengren: *J. Mech. Phys. Solids,* 1968, vol. 16, pp. 1-12.
26. J.W. Hutchinson: *J. Mech. Phys. Solids,* 1968, vol. 16, pp. 13-31.
27. M.F. Ashby: *Phil. Mag.,* 1970, vol. 21, pp. 399-424.
28. L.M. Brown and W.M. Stobbs: *Phil. Mag.,* 1976, vol. 34, pp. 351-72.
29. L.M. Russell and M.F. Ashby: *Acta Metall.,* 1970, vol. 18, pp. 891-901.
30. J. Gurland: in *Quantitative Microscopy,* R.T. DeHoff and F.N. Rhines, eds., McGraw-Hill, New York, NY, 1968, p. 279.
31. J.W. Cahn and J. Nutting: *Trans. ASME,* 1959, vol. 215, p. 526.
32. J.D. Edington: *Practical Electron Microscopy in Materials Science,* Van Nostrand Reinhold Company, London, 1976, p. 207.
33. T.H. Sanders, Jr. and E.A. Starke, Jr.: *Metall. Trans. A,* 1976, vol. 7A, pp. 1407-18.
34. T. Kawabata and O. Izumi: *Acta Metall.,* 1981, vol. 29, pp. 229-39.
35. G. Lütjering and A. Gysler: in *Aluminum Alloys: Their Physical and Mechanical Properties,* E.A. Starke, Jr. and T.H. Sanders, Jr., eds., E.M.A.S. West Midlands, England, 1986, p. 1547.
36. J.R. Low, Jr.: *Eng. Fract. Mech.,* 1968, vol. 1, pp. 47-53.
37. R.H. Van Stone, T.B. Cox, J.R. Low, and J.A. Psioda: *Int. Met. Rev.,* 1985, vol. 30, pp. 157-78.
38. S.H. Goods and L.M. Brown: *Acta Metall.,* 1979, vol. 27, pp. 1-15.
39. B.I. Edelson and W.M. Baldwin, Jr.: *Trans. ASM,* 1962, vol. 55, p. 230.
40. P.F. Thomason: *J. Inst. Met.,* 1968, vol. 96, p. 360.
41. K. Komori: *Acta Mater.,* 1999, vol. 47, pp. 3069-77.
42. S.E. Urreta, F. Louchet, and A. Ghilarducci: *Mater. Sci. Eng. A,* 2001, vol. A302, pp. 300-07.
43. K. Tanaka, T. Mori, and T. Nakamura: *Phil. Mag.,* 1970, vol. 21, pp. 267-79.
44. J. Sun: *Int. J. Fract.,* 1990, vol. 44, pp. R51-6.
45. S.L. Lee and S.T. Wu: *Metall. Trans. A,* 1986, vol. 17A, pp. 833-41.
46. M.A. Zaida and T. Sheppard: *Met. Technol.,* 1984, vol. 11, pp. 313-19.
47. G.T. Hahn and A.R. Rosenfield: *ASTM STP432,* ASTM, New York, NY, 1968, pp. 5-32.
48. D.E. Osborne and J.D. Embury: *Metall. Trans.,* 1974, vol. 4, pp. 2051-61.
49. W.H. Tai: *Mater. Sci. Eng. A,* 1989, vol. A123, pp. 205-10.